Journal Title
XX(X):1–39

DOI: 10.1177/ToBeAssigned
www.sagepub.com/
SAGE

Analysis of temperature and altitude effects on the global energy balance during WLTC

Francisco Payri, Jaime Martín*, Francisco J. Arnau and Sushma Artham

Abstract

In this work, the Global Energy Balance (GEB) of a 1.6 L compression ignition engine is analysed during WLTC using a combination of experimental measurements and simulations, by means of a Virtual Engine. The energy split considers all the relevant energy terms at two starting temperatures (20°C and 7°C) and two altitudes (0 and 1000 meters). It is shown that reducing ambient temperature from 20°C to -7°C decreases brake efficiency by 1 % and increases fuel consumption by 4 %, mainly because of the higher friction due to the higher oil viscosity, while the effect of increasing altitude 1000 m decreases brake efficiency by 0.8% and increases fuel consumption by 2.5% in the WLTC mainly due to the change in pumping. In addition, GEB shows that ambient temperature is affecting exhaust enthalpy by 4.5%, heat rejection to coolant by 2% and heat accumulated in the block by 2.5%, while altitude does not show any remarkable variations other than pumping and break power.

Keywords

Transient, Global Energy Balance, Virtual Engine, WLTC, Cold-start, Altitude, Ambient

Corresponding author:
Martín Díaz Jaime, CMT-Motores Térmicos, Universitat Politècnica de València, Camino de Vera s/n. 46022 València, Spain, www.cmt.upv.es, Tel: +34963877650, fax: +34963877659
Email: jaimardi@mot.upv.es

Prepared using sagej.cls *[Version: 2017/01/17 v1.20]*

Nomenclature

ACS	Ambient cold start
CI	Compression ignition
DI	Direct injection
ECU	Engine control unit
EGR	Exhaust gas recirculation
GEB	Global energy balance
HPEGR	High pressure exhaust gas recirculation
HSDI	High speed direct injection
ICE	Internal combustion engines
IMEP	Indicated mean effective pressure
LPEGR	Low pressure exhaust gas recirculation
LTCS	Low temperature cold start
NEDC	New european driving cycle
1D	One-dimensional
VEMOD	Virtual engine model
WLTC	World harmonized light vehicles test cycle
WLTP	World harmonized light vehicles test procedure
0D	Zero-dimensional

Introduction

For decades, CI engine has dominated market because of their fuel efficiency and reliability. They have been extensively used in the transport sector whose development is aimed at achieving high efficiency [1,2] and low emission [3,4]. Nowadays, CI engines have to face challenges including improved thermal efficiency and real driving emissions [5,6]. In fact, important efforts have been made in the recent years to improve the combustion, emissions and performance of CI engine, mainly in warmed conditions [7–10].

Engines are mostly used under transient conditions and only a small proportion of daily driving schedules involve steady-state operation [11]. When compared to the steady-state conditions, the transient operation is closer to the real-world engine operation and thus, new driving cycles are based on this operation mode [12,13]. The global concern regarding environmental pollution has led to the increase in the interests on transient operation and real driving emissions, which led to the World harmonized Light vehicles Test Procedure (WLTP) [14]. It came into force in September 2017 in Euro 6d-Temp and has more realistic testing conditions, including the extended ambient temperature ranges covering low temperature operation [15] . WLTC has forced the automotive industry to optimize different technologies [15,16], but research in transient operation is still limited when compared to the steady-state operation. However, different engine phenomena still require improving predictive modelling performance in transient, beyond the results extrapolated from steady-state conditions [17–19].

When considering the engine behavior in transient operation, ambient, coolant and oil temperatures, are important as they affect the heat rejection and in-cylinder conditions, thus affecting combustion, emissions formation and mechanical losses. Moreover, usually engine calibration changes according to the coolant and oil temperatures[20]. Because of the dramatic spatial and temporal thermal variation, the initial stage after the cold starting is one of the most important transient processes of CI engines. Moreover, low ambient temperatures during start process have a notable influence on the combustion process [21–23]. Research on cold-start in CI engines have shown that emissions tend to increase when ambient temperature diminishes[6,24]. Also, low ambient temperature leads to enhance incomplete combustion[6,25,26]. Fuel consumption also increases with the lower combustion efficiency and higher mechanical losses[6]. The reduction of cold start emissions in CI engines has become an increasingly important issue, because the fuel consumption and exhaust gas emissions associated with cold-start conditions are higher than those associated with warmed engine conditions[6,27]. Due to the regulations requirement, cold-start has received the attention of the researchers, in particular engine operation under WLTC and real driving emissions [24,28–33]. Some researchers focused on the cold start performance of CI engines and had investigated the impacts of exhaust gas recirculation on engine performance[28–30,33–36]. Thus, Christos Dardiotis et al.[24] experimentally investigated CO, HC and NOx emissions of Euro 4/5/6 CI passenger cars at low temperature of -7°C based on the cold start driving cycle, whose research results proved emission pollutants increased remarkably at low temperature (-7°C) compared to the ambient test. Apart of temperature conditions, altitude is a second key issue affecting engine operation. Liu et al.[37] investigated the change of intake oxygen content caused by altitude variation and its affect on the performance of CI engines. They found that the brake specific fuel consumption (BSFC) decreases with the increase of atmospheric pressure.

Reduction of consumption and emissions requires evaluating new strategies in the transient operation. In this framework, Global Energy Balance (GEB)[38,39] is a useful approach for the assessment of parameters affecting engine consumption. Various paths followed by the chemical energy can be identified and quantified using GEB. A simple energy balance can be carried out by considering the fuel power, brake energy, heat transfer, mechanical losses and the exhaust gas energy. Some works dealing with experimental and theoretical energy balance can be found in the literature[40–43]. Abedin et al.[41] did a thorough study on GEB using various alternative fuels[42] and determining the key variables effecting GEB and performance of the engine. In few previous works, various injection strategies at different operating conditions were studied with the help of the analysis of energy repartition[40,44,45]. The energy balance can be performed in a more detailed way by considering the heat transfers to the coolant and oil[44]. The neglected terms that account for energy losses with minor impact include unburnt fuel, heat rejection to the ambient and blow-by enthalpy[46].

In order to perform the engine thermal balance in detail, 0D/1D simulation tools have a large potential, as showed at[43,47,48]. Also the combination of experiments and theoretical analysis provides a deep insight in the key issues controlling the energy degradation in the engine as shown in two previous works [43,47–49].

Steady-state conditions are the main focus in most of the described publications and thus, very few works can be found dealing with the analysis of energy balance in transient operation[50], and with the effect of ambient conditions, including the temperature or altitude[51]. Moreover, the few available works do not offer a deep analysis of the energy balance from experimental or modeled point of views. This leaves a gap in the engine research that this work tries to cover.

The first contribution is the methodology used to perform the analysis of the energy balance by combining experimental and simulated information. On the one hand, experimental fluid temperatures are used to validate the model performance, while some experimental settings (such as instantaneous fuel and air mass flows) are imposed as targets, for the engine control, during simulations. On the other hand, detailed simulated energy split is assessed along WLTC by means of a 0D/1D tool called VEMOD. The tool, once validated in cold conditions (validation in ambient conditions was carried out in a previous work[52]), provides information that is hard or even impossible to obtain experimentally such as, among others, the heat rejection to different engine parts or the mechanical loses split.

A cumulative approach has been applied to plot the energy terms along WLTC, thus each of them has been averaged from the start until a determined instant to provide a mean transient evolution. Although not conventional in other works, this approach is necessary to avoid the excessive noise of raw instant evolution.

The second main contribution of the work is the results and discussion on the effect of ambient temperature and engine altitude on the GEB in transient operation in a 1.6 L CI engine. Thus, two starting temperatures, 20°C (Ambient Cold Start -ACS-) and -7°C (Low Temperature Cold Start -LTCS-) and two altitudes (0 and 1000 meters), both at LTCS are considered. The analysis is performed, on the one hand, discussing the instantaneous evolution of the energy terms at different conditions, justifying the observed trends, and highlighting the most interesting differences along WLTC. On the other hand, a final comparison of the total cumulated terms, at the end of WLTC, allows providing a clear summary of the main effects. For the sake of clarity, the analysis includes some in-cylinder and combustion parameters, and finally NOx emissions.

The work is organized in different sections devoted to firstly describe the experimental and modeling tools, followed by the methodology description. Thereafter, a brief description of the Global Energy Balance and the model validation is provided. Then the GEB discussion for different ambient conditions is carried out, finishing the work with the most relevant conclusions in the last section.

Experimental and modeling tools

Experimental tool

The research was carried out in a multi-cylinder, HSDI Diesel engine. The engine is a 1.6L four-stroke Euro 6 compliant engine. The specifications of the engine can be seen in Table 1.

Table 1. Engine specifications

Type	**HSDI Diesel engine**
Displacement	1598 cm³
Bore	80 mm
Stroke	79.5 mm
Compression ratio	15.9:1
Number of valves	4 / cylinder
Number of cylinders	4
Air management	VGT, HP-EGR, LP-EGR
Maximum power @ speed	96 kW @ 4000 rpm
Maximum torque @ speed	320 Nm @ 1750 rpm
Engine oil	0W-30
Engine coolant	50% glycol-50% water

The test cell as shown in Figure 1, is fully equipped to measure main operation mean variables (e.g. air and fuel mass flows, temperature and pressure at intake and exhaust lines, etc.), some liquids (oil and coolant) temperatures, coolant mass flows and in-cylinder pressures in the four cylinders. Table 2 summarizes the relevant instrumentation used for this study.

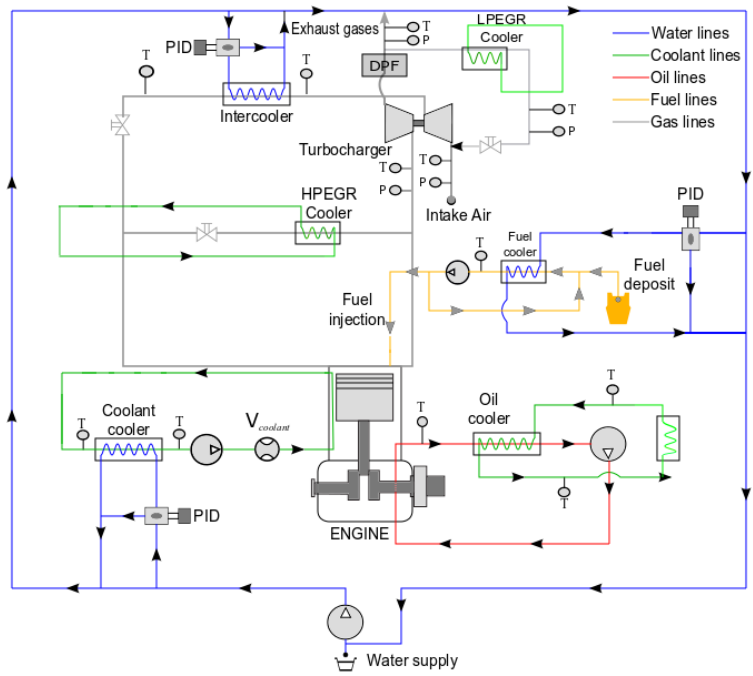

Figure 1. Test cell scheme

Table 2. Test cell instrumentation

Variable	Instrument	Range	Accuracy
Crank angle	Encoder	0-360°	±0.02°
Torque	Dynamometer	0-400 Nm	±0.5 Nm
Gas temperature	k-type thermocouple	70-1520 K	±2 K
Air mass flow	Sensyflow DN80	0-1700 kg/h	±2 %
Coolant flow	Krohne 4010 Optiflux	4.5-90 L/min	±0.5 %
Oil pressure	Piezoresistive transducer	0-10 bar	±25 mbar
In-cylinder pressure	AVL GH13P	0-200 bar	Linearity 0.3%

The steady-state tests for calibration were performed at 26 operating points. They cover a wide range of the engine map and testing points belonging to the WLTC as shown in Table 3.

Table 3. Steady-state tests performed

Engine speed in rpm	Load in %
1000	Motoring
2000	Motoring
3000	Motoring
4000	Motoring
850	idle
1000	21, 44, 66, 88
1250	13, 26, 50, 76, 100
1500	11, 25*, 50, 75*, 100
2500	25, 50, 75, 100
3500	25*, 50, 75, 100

* Both conventional (20°C) and cold ambient conditions (-7°C)

The test bench in which the engine is installed includes a control of ambient temperature and also of the temperature of the water in a large reservoir. This water is used to cool down the intercooler, fuel and coolant. In the case of LTCS, the water temperature is at -7°C and in the case of ACS, it is around 20°C. The control of the coolant temperature, which is a key parameter for thermal performances, is carried out automatically through the engine thermostat, thus mimicking real operation. The coolant temperature is around 85 ± 5°C in hot conditions. In the case of motoring tests, the temperature of the coolant will stabilize at a determined temperature that depends on the engine speed.

To measure and simulate WLTC, the instantaneous load and engine speed was obtained from the vehicle speed profile of a vehicle class 3 (W/kg>>34), which is a multi-purpose vehicle, powered by the 1.6 L Diesel engine. The transient analysis is performed in three WLTC tests, measured with ACS and LTCS conditions (starting at -7°C) at 0 m. Table 4 summarizes the different engine temperatures at these conditions at the beginning of the test. Three repetitions of each steady-state point and WLTC were measured.

Table 4. Initial temperatures in the WLTC tests performed

Test conditions	Room temperature	Initial block temperature	Initial Coolant temperature	Initial Oil temperature
ACS	20°C	20°C	20°C	20°C
LTCS	-7°C	-7°C	-7°C	-7°C

Predictive tool

The Virtual Engine Model (VEMOD)[15] is a home-developed standalone tool aimed at simulating new standard testing cycles. It covers the calculation of different processes as outlined in Figure 2, where the sub-models included are summarized. The entire

sub-models used are shown in Figure 2. The 1D gas dynamics model computes air management and by means of explicit sub-models, it is able to calculate the processes in all the engine components such as heat exchangers, turbocharger, aftertreatment systems etc. The gas dynamics model is combined with a cylinder model that predicts in-cylinder conditions taking into account the injection-combustion process. The whole set of sub-models, marked with a blue box in Figure 2, make up the engine model[15]. The red boxes in Figure 2 represent the various control sub-models. They have been developed in Matlab/Simulink[15]. The control sub-model allows controlling the operating points (during steady-state and transient conditions) of the engine model. The vehicle dynamics model allows calculating the instantaneous vehicle velocity taking into account the engine torque, road characteristics and driver behavior. However, as in this study the focus is put on the engine performances, the vehicle calculation has been omitted by imposing the engine speed and target torque to follow the WLTC.

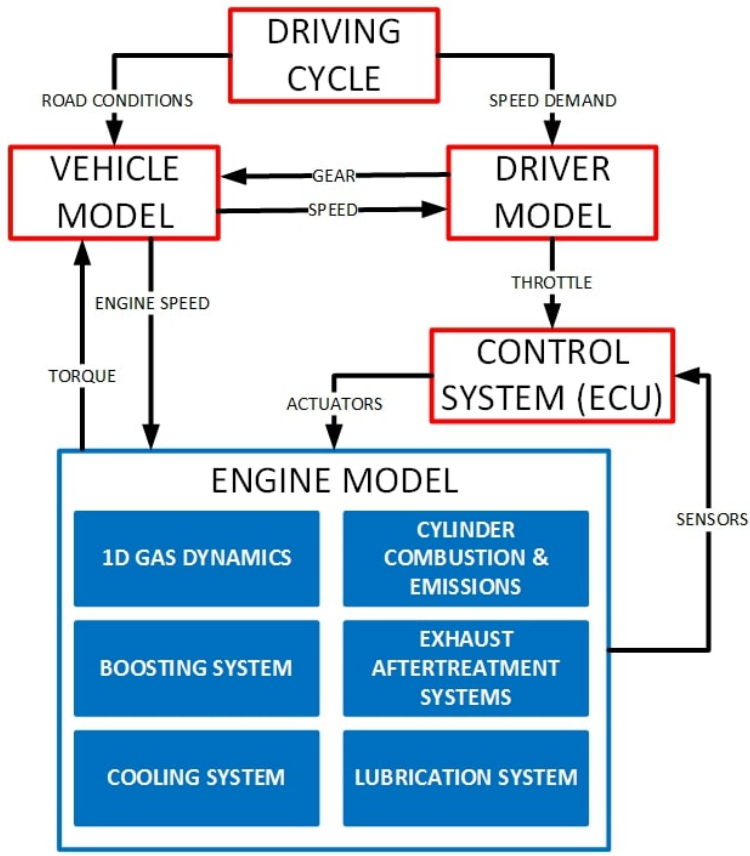

Figure 2. Flow-chart of Virtual Engine Model (VEMOD) subsystems

Steady-state operating points can be simulated by VEMOD without the control system sub-model, by imposing the target value of actuator, in the engine model. Whereas, for transient operation, control system sub-model is needed to follow certain targets by acting on the different actuators related to air management (turbine rack position, EGR valve...) and injection settings (pressure and injection timing and fuel mass injected in each pulse). Virtual ECU allows mapping the injection settings as a function of speed and fuel mass. Different energy terms will be modelled to complete the energy balance of the system using VEMOD.

Combustion diagnosis tool

A combustion diagnosis tool called CALMEC[38,53], developed at CMT-Motores Térmicos was used to calculate the heat release and to calibrate the in-cylinder heat transfer in VEMOD[53–55], based on the experimental measurements in steady-state conditions as described in [54].

Methodology

The scheme of the methodology followed is shown in Figure 3. It was structured as follows:

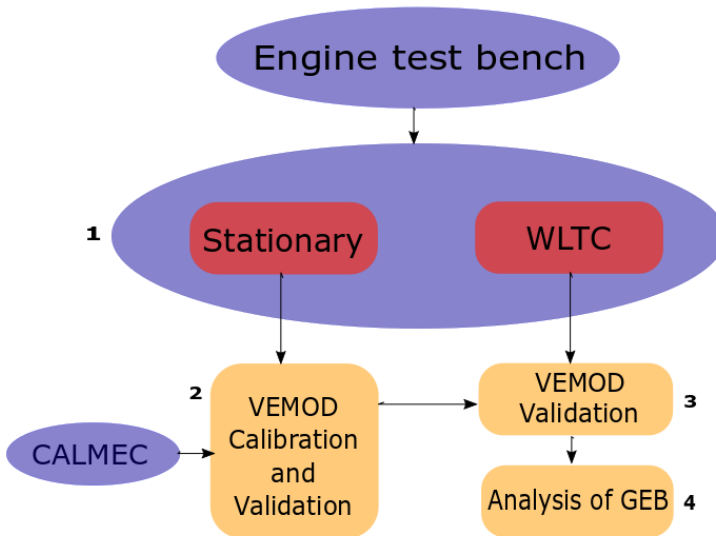

Figure 3. Methodology

1. The steady-state and WLTC transient tests were measured in the installation described in the experimental tool section. The parameters required for the analysis (engine speed, torque, air and fuel mass flows, oil and coolant temperatures,

temperature and pressure at intake and exhaust lines, coolant mass flows and in-cylinder pressures in the four cylinders) were measured as described.

2. Calibration of the combustion sub-models[15], in-cylinder heat transfer[54] and mechanical losses[38] were carried out using the set of steady-state points. As the results were presented in Olmeda et al[52], a brief description of the results is included to avoid reccurence.

3. The VEMOD validation in various transient tests is performed by comparing simulated WLTC cycle with experimental result. The validation was performed using experimental data of the evolution of fluid temperatures and brake torque.

4. An extensive analysis of the energy repartition was carried out to assess the effect of different variables on the Global Energy Balance (GEB) and engine performance. GEB during WLTC was obtained at different altitudes (0 m and 1000 m) and thermal conditions, using some experimental data to set target conditions during simulation, as detailed below.

For the calculation of both steady-state points and WLTC, the experimental values of the torque, air mass flow and boost pressure were set as targets and the injection settings and engine speed were directly imposed along the cycle.

Global Energy Balance (GEB)

The basis of the analysis is the first law of thermodynamics. Different paths followed by energy terms are represented in Figure 4, where all the energy transformations taking place in a turbocharged engine are considered [38,39,52,56,57].

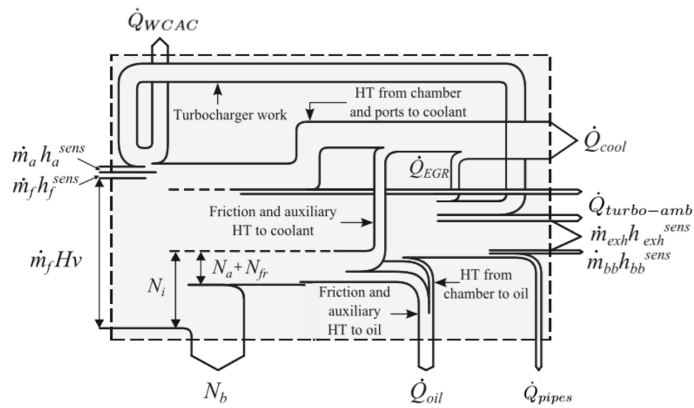

Figure 4. Schematic representation of GEB

The energy flows entering the engine are the sensible enthalpy of air $\dot{m}_a h_a^{sens}$, the sensible enthalpy of fuel $\dot{m}_f h_f^{sens}$ and the chemical energy of the fuel $\dot{m}_f H_v$. The

outlet energy flows are the brake energy N_b, the power to run auxiliary elements[58] N_a, the heat flow to the coolant[59,60] $\dot{Q}_{cool}$, the flow of sensible enthalpies of the exhaust gases $\dot{m}_{exh}h_{exh}$, the heat rejection to oil[59] $\dot{Q}_{oil}$, the heat cumulated in the engine block $\dot{Q}_{mat}$, the heat rejection in the intercooler $\dot{Q}_{WCAC}$, the heat rejection in the EGR heat exchangers, $\dot{Q}_{LPEGR}$ and $\dot{Q}_{HPEGR}$, the heat from the external walls of the engine to the ambient due to the heat rejection in the pipes $\dot{Q}_{pipes}$ and turbo case[59,60] $\dot{Q}_{turbo-amb}$, and finally the enthalpy flow of blow-by losses, H_{bb}[38,39,56].

In order to perform the detailed analysis of energy repartition, sensible enthalpy terms are rearranged to obtain the net flow of sensible enthalpy, H_{exh}, determined by means of a balance between the enthalpy flow of incoming air and fuel and outgoing exhaust gases. Thus, the first law of thermodynamics can be expressed as:

$$\begin{aligned}\dot{m}_f H_v =& N_b + N_a + H_{exh} + \dot{Q}_{cool} + \dot{Q}_{oil} + \dot{Q}_{mat} + \dot{Q}_{WCAC} + \dot{Q}_{HPEGR} \\ &+ \dot{Q}_{LPEGR} + \dot{Q}_{pipes} + H_{bb} + \dot{Q}_{turbo-amb}\end{aligned} \tag{1}$$

More details about the terms and how they are determined in the GEB analysis is explained in Olmeda et al[52].

Model calibration and validation

Calibration in steady-state conditions

In order to proceed with the analysis of energy balance, the calibration of the Virtual Engine, VEMOD, was previously performed. The calibration includes the determination of the fitting constants of different sub-models of VEMOD. It was performed using motoring tests, which were used to perform an initial convective heat transfer tuning and combustion tests, which were used for commissioning the rest of sub-models, in steady-state conditions. Experimental matrix used for the calibration is detailed in Table 3.

Experimental heat release is the main source of information for combustion model calibration; however, it is affected by the heat transfer rejection. Thus, the combustion model calibration was performed after the calibration of the heat transfer model. The combustion model is composed of three main sub-models: ignition delay, premix combustion and diffusion combustion models; along with a 1D model describing the mixing process. The approach for the mixing process, key issue for both the heat release and emissions predictions, is a physical model based on the turbulent gas jet theory[61]. The ignition delay (ID) model is based on a simplification and parameterization of a complete n-heptane chemical kinetics description from[62]. The premixed combustion model is an empirical model based on the propagation velocity of a premixed flame that considers in-cylinder conditions (pressure, temperature and composition). The diffusion combustion phase is assumed to be mixing controlled: the fuel mass in each fuel parcel will be burned when it reaches stoichiometric conditions, and mixing model determines when these conditions are reached. It is necessary to indicate that to achieve an accurate prediction of the diffusion combustion, quasi-steady conditions and transient processes at the start and end of the injection are considered separately. The calibration of the

combustion model includes the determination of the different constants of the three sub-models. The criterion for the determination of the sub-model fitting constants was to minimize the difference between the experimental heat release and the simulated one.

The detailed description of the calibration can be found in the previous work of Olmeda et al[52]. Some brief results can be seen in Figure 5. Top two plots of Figure 5 show the experimental and modeled heat release at engine speed of 2500 rev/min at different loads (25% and 100%). The dotted lines represent the modeled values from VEMOD for one cylinder and the solid lines represent the experimental values of the four cylinders. As shown, the heat release evolutions are quite well predicted and the discrepancy is, in general, similar to differences between cylinders. Bottom two plots of Figure 5 represent the heat release at engine speeds of 1250 and 3500 rev/min and load of 50%. Also, a good global agreement of modeled vs experimental results can be seen. It can be highlighted that the modeled heat release is slightly slower than the experimental ones at high speed and load. The reason for the slightly poorer performance at these conditions is because the focus was put on the low-mid ranges because they are critical for the WLTC simulation, main objective of the work. In the previous work of Olmeda et al[52] the pressure and heat release evolutions at various speeds and loads were shown in detail, they have been omitted here for the sake of brevity.

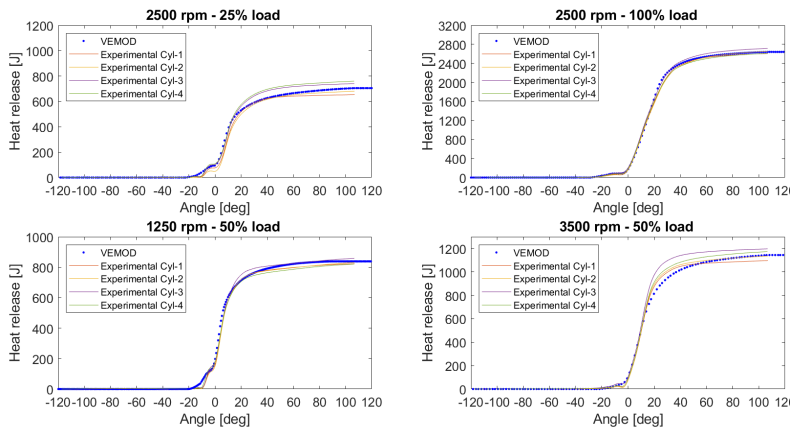

Figure 5. Heat release at different loads (top) and speeds(bottom) in steady-state conditions.

The analysis was extended to other key outputs in the complete engine map such as IMEP, with a mean error about 3%, turbine inlet temperature, with a mean error of 2.5% and coolant temperature, which mean error is 0.5%. In any case, the global performance of the model was shown to be good, with a slightly higher uncertainty at high load conditions that are less critical for WLTC simulation.

Transient validation of at low temperature cold start

In order to ensure the good performance of the model in transient conditions before performing the energy balance, the validation at low temperature cold start (at -7°C) is presented in this section. Validation at ambient cold start (at 20°C) was presented in a previous work[52]. As mentioned in the methodology section, the experimental speed and torque, injection settings, air demand and boost pressure are set as targets for the control system during the WLTC, while brake torque and some key temperatures of gas and liquids circuits are compared with their experimental values to check the model performance.

Tests performed at ambient conditions by Olmeda et al[52] were conducted with engine settings calibrated for Euro 5 regulation. In that calibration, no EGR strategy is applied until almost half of the cycle for low temperature start. However, in this work, calibration has been updated in order to face upcoming Euro 7 regulation. Thus, in the current calibration high pressure EGR is used from the very beginning, to promote the increase of inlet temperature and later, when coolant temperature reaches 80°C, low pressure EGR strategy is applied.

For the sake of brevity, the following four relevant variables are shown for validation in Figure 6 to Figure 8 : torque, turbine outlet temperature, coolant and oil temperatures.

Figure 6 shows the torque and cumulated brake energy during a complete WLTC, starting at -7°C. It can be seen that the evolution of the torque is well followed by the model, in particular during the fast load changes. The torque prediction has a mean error of 10 Nm (mean relative error is about 7%), having 90% of the total points an error below 11 Nm. Even though some discrepancy can be observed at the low load variations, the cumulative effect at the end of the complete cycle is only 4%.

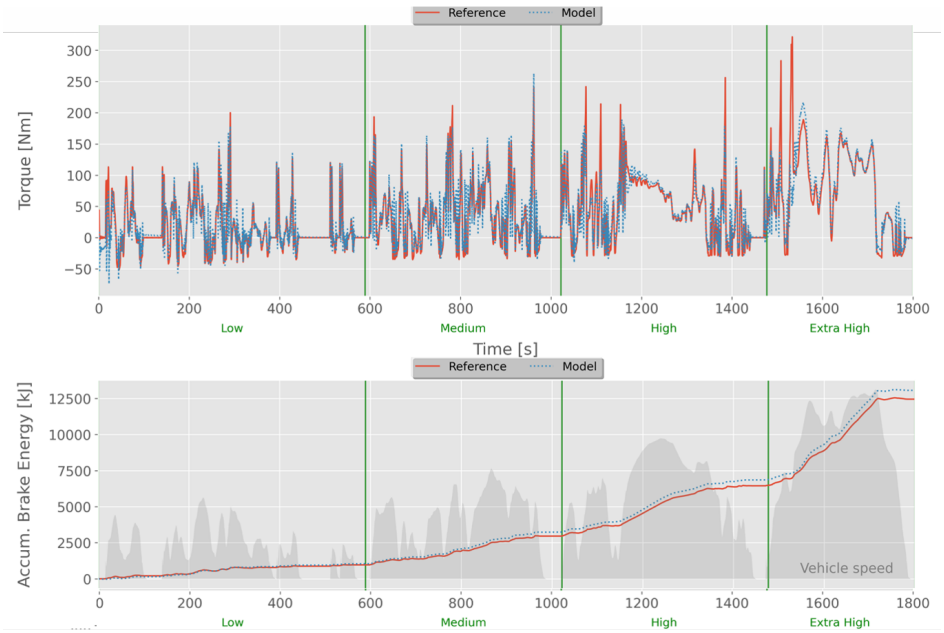

Figure 6. Brake torque and brake energy in transient at LTCS conditions

Figure 7 and Figure 8 shows the coolant and oil temperature in transient conditions, key parameters to track the thermal performance of the engine in low temperature conditions. The mean error of the coolant temperature is 3°C and the relative error is 1%. Whereas, the mean error of the oil temperature is 4°C and the relative error is about 1.5%. Also, 90% of points show relative error below 6°C for both coolant and oil temperatures, which shows a good model prediction. The good performance of the coolant and oil temperatures allow ensuring the accuracy of heat rejection prediction, key issue in the energy balance in low temperature conditions. Results at ambient cold start conditions have been omitted for the sake of brevity, but they are pretty similar to those shown for low temperature cold start and even though with a different calibration, Euro7 target vs Euro 5, also similar to those reported by Olmeda et al.[52] in ambient conditions.

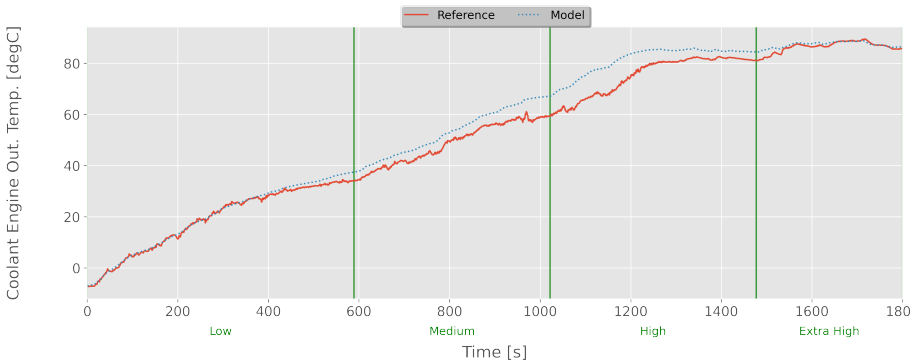

Figure 7. Coolant temperature in transient at LTCS conditions

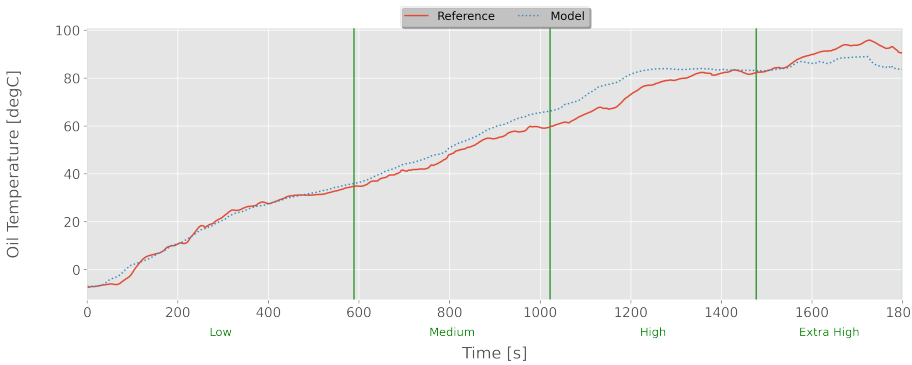

Figure 8. Oil temperature in transient at LTCS conditions

GEB analysis

It is interesting to provide an initial discussion before starting with the GEB analysis. If the energy balance was performed in steady-state conditions, the addition of all the energy flows would provide a residual close to zero, and only an small unbalance would remain due to some experimental uncertainty[54](if analysis is based on measurements) or numerical error. However, as detailed in a previous work[52], a "delay" phenomenon have to be considered in the energy balance during transient conditions. System response is almost instantaneous when the engine cylinder and ports are considered for the energy balance. If the complete engine including heat exchangers and all the gas lines are considered, there is an apparent inconsistency between the instantaneous heat release in the cylinders due to the combustion process (main term at the left in Equation (1) and main input for the GEB) and the addition of the rest of energy terms. This inconsistency tends to be negligible when the enthalpy is integrated during a long time, as discussed below.

In the GEB analysis, the cumulative energy terms are plotted by integrating the power of each term and dividing it by the the cumulated fuel energy until a determined instant.

Low temperature cold start conditions

Figure 9 shows the energy balance considering the complete engine during WLTC starting at -7°C. The analysis includes all the elements from engine inlet (ambient conditions) to the exhaust. As stated, there is an apparent unbalance from the beginning of the cycle. Thus, there is no perfect agreement between the input fuel energy and the addition of the exhaust energy, brake energy, auxiliary power, heat transfer to coolant, oil, cumulated heat in the material, heat rejected at high pressure and low pressure EGR coolers, WCAC (intercooler) and to the ambient. As justified, this can be explained because of the non-synchronized phenomena taking place in the pipes and the in-cylinder leading to a delay in the calculation of the enthalpy flows, that causes a global lag of energy at the beginning. This effect diminishes as the time increases and is small at the end of the WLTC, after 1800 seconds, where the total cumulated energy reaches 85% of the injected energy. However, when the cycle is extended and run for a longer time, energy balance tend to stabilize gradually to reach the agreement of about 100% between input and output energies of engine. This can be seen in Figure 10, where simulation has continued after the WLTC, repeating the cycle until 5700 s. This effect is similar at ambient cold start conditions, where the total cumulated energy reaches about 86% of the injected energy, after 1800 seconds and stabilizes gradually when the cycle is extended.

In Figure 9, at the end of cycle, brake energy, N_b constitutes about 29% of total fuel energy (mean brake efficiency of 29%). However, it is clearly lower during initial operation and increases during the second part of the cycle, where engine operates at higher loads. This can be justified because of the large mechanical losses and the high amount of energy rejected to the walls and used to heat the metal and liquids at the beginning of the cycle, because of the low initial temperatures. The heat rejected to coolant ($\dot{Q}_{cool}$), oil ($\dot{Q}_{oil}$) and material ($\dot{Q}_{mat}$) contribute about 30% of the total energy output at the end of the cycle. However, initially, $\dot{Q}_{mat}$ is the most important term,

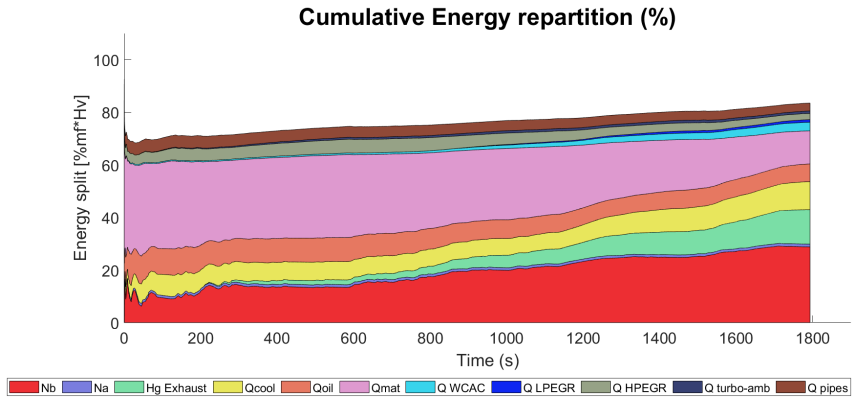

Figure 9. Total cumulative energy repartition in WLTC at LTCS conditions

reaching about 50% of total energy because of the block temperature during the initial operation is cold. As the metal and fluids temperatures increase, the power used to heat the block tends to reduce. A slight increase in the heat rejected to coolant ($\dot{Q}_{cool}$) was obtained from around 1200 seconds on, because of the thermostat opening. $\dot{Q}_{cool}$ is quite stable and slightly lower to 7% until this point. However, at 1250 seconds the value starts to be higher to 7% and a continuous increase takes place until 1800 seconds, when $\dot{Q}_{cool}$ is about 11%. $\dot{Q}_{oil}$ is slightly higher at the first half of the cycle due to the higher friction losses at the beginning, due to the lower oil temperature. $\dot{Q}_{oil}$ is about 7% at the end of the cycle.

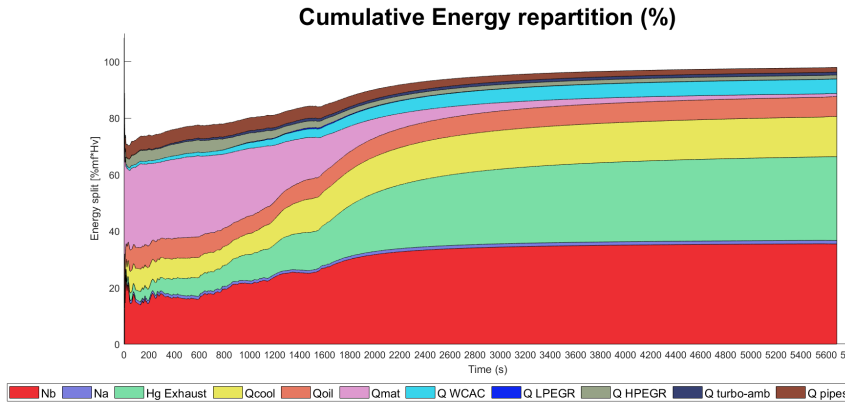

Figure 10. Extended cycle of Total cumulative energy repartition in WLTC

The net exhaust enthalpy, $H_{g,exhaust}$ (calculated between engine intake and downstream the low pressure EGR pipe), contributes about 13% of total engine energy output at the end of the cycle. A trend to increase $H_{g,exhaust}$ can be seen in the second half of the WLTC mainly due to the higher load and speed during the high and extra-high parts of the cycle but also due to the progressive reduction of the relative effect of heat accumulation in the block[56]. Cumulated heat rejected to the intercooler is about 4% of the fuel energy, being negligible until 500 seconds after cycle beginning due to the small difference of the air temperature between the compressor outlet and the intercooler coolant because of the low boost pressure in this part of the cycle. HPEGR and LPEGR loops are activated depending on the coolant temperature, thus LPEGR is activated when coolant reaches 70°C. At the end of the cycle only about 4% of the total energy is rejected in the EGR coolers. About 4% of heat is rejected to ambient through turbocharger and pipes ($\dot{Q}_{turbo-amb}$ and $\dot{Q}_{pipes}$).

Going deeper in the analysis of the efficiencies, Figure 11 shows the percentage of accumulated indicated and brake energies at LTCS conditions along the WLTC. Indicated energy ranges from 40% at the beginning to 44% at the end of the cycle, while brake energy ranges from about 10% at the WLTC start to 29% at the end, showing a clear trend to increase with time. Having in mind that indicated efficiency is not affecting dramatically brake efficiency, its evolution must be understood by analysing mechanical losses that are shown in Figure 12.

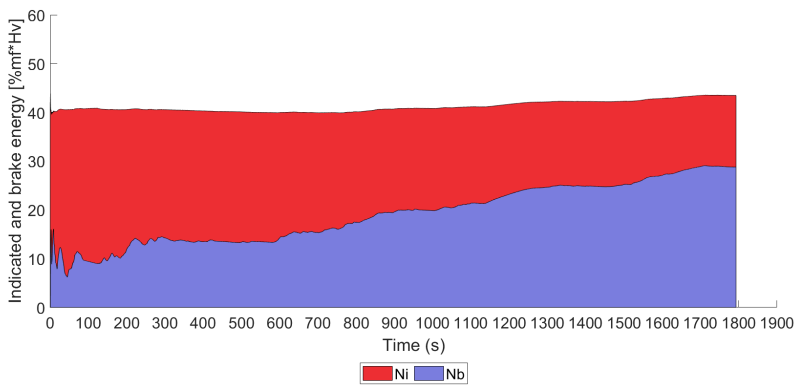

Figure 11. Cumulative indicated and brake energies in WLTC at LTCS conditions

Top of Figure 12 shows that there is a large reduction of the mechanical losses weight, in particular due to the friction, reaching about 30% of the fuel energy at the start of the WLTC and diminishing to 11% at the end of the cycle, while pumping (N_p) is only about 3% and auxiliaries (N_a) are 1% both of them with a negligible variation along the cycle. Having a look to these results, the lower values of brake energy at the beginning of the operation can be explained by the higher mechanical losses, because of low coolant and thus oil temperatures during the beginning of the operation, thus affecting the oil viscosity.

As shown in the bottom of Figure 12, piston friction, N_{fr} piston, is the main component of the friction. It is about two thirds of the total friction (7% of the fuel energy). Bearing friction has the intermediate contribution and the valve train is the less important one among all the three. This friction repartition is consistent with some previous analysis performed in steady-state conditions [56].

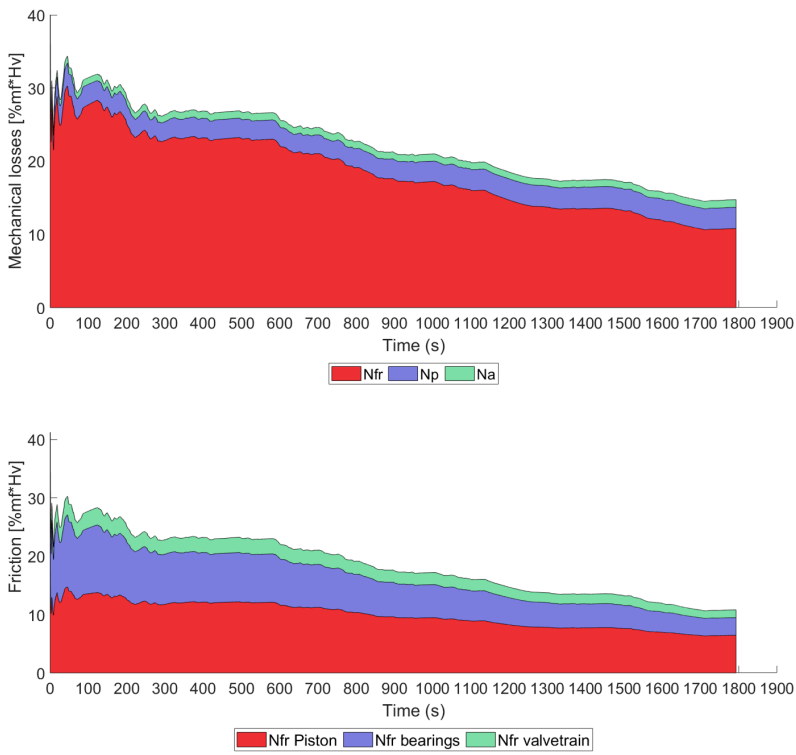

Figure 12. Cumulative mechanical losses (top) and friction split (bottom) in WLTC at LTCS conditions

Ambient cold start conditions

Main purpose of this work is to compare the energy split starting at LTCS conditions with ACS conditions, which energy balance considering the complete engine can be seen in Figure 13. At a first glance, Figure 9 and 13 are similar, but a deeper analysis will show differences in detail, specially for brake efficiency and exhaust enthalpy that are quite different, in particular during the first half of the cycle. N_b at the beginning of WLTC is clearly higher with ACS (about 25%) than with LTCS (about 15%). As shown in Figure 14 and 15, even though the indicated efficiency during first half of the WLTC is slightly lower to LTCS (39% vs 40%), the differences in N_b has to be majorly attributed to mechanical losses that are comparitively lower in ACS as shown in Figure 15. When comparing Figure 15 and top figure in Figure 12 it can be concluded that the difference is mainly due to the friction term, up to about 10% of the fuel energy higher at LTCS at the beginning of the WLTC; even though this discrepancy is later reduced.

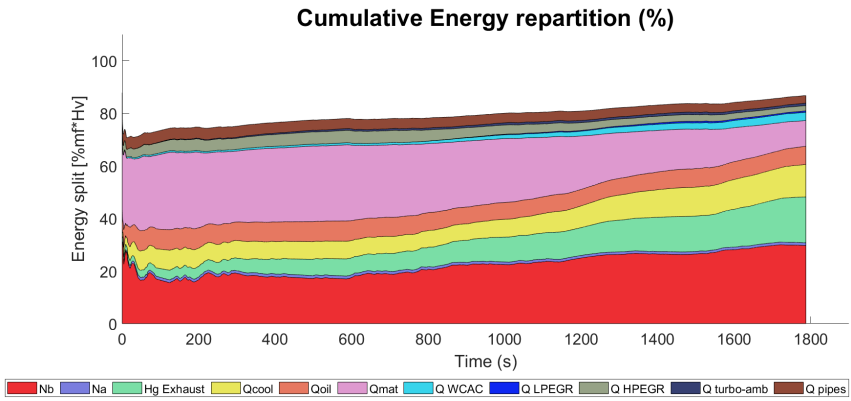

Figure 13. Total cumulative energy repartition in WLTC at ACS conditions

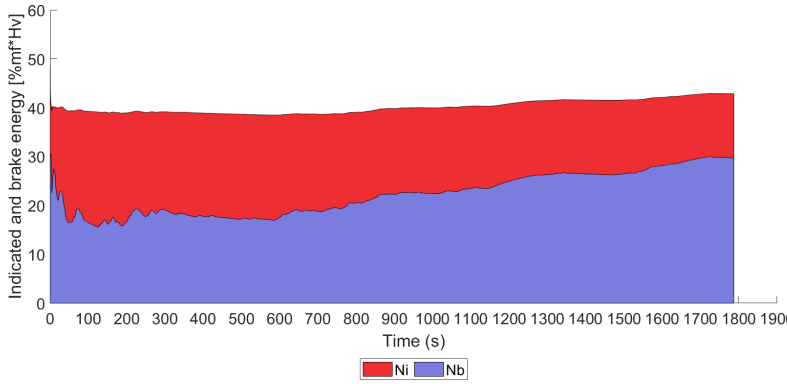

Figure 14. Cumulative indicated and brake energies in WLTC at ACS conditions

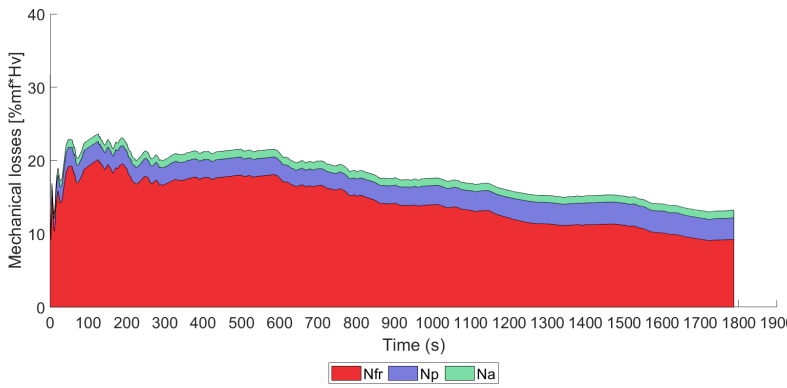

Figure 15. Cumulative mechanical losses in WLTC at ACS conditions

The comparison of energy terms at the end of the WLTC in LTCS and ACS at an altitude of 0 m, is summarized in Figure 16. The first change when comparing with results starting at LTCS conditions can be seen in the brake energy, which is about 30% in ACS conditions, 1% higher than in LTCS. This can be mainly explained because of the higher mechanical losses in LTCS, that is partially compensated by indicated efficiency, which is also higher, as seen in the Figure 17, where friction is about 9% in ACS (2% lower than in LTCS) and N_i is about 43%. It is interesting to highlight that Ni during ACS is 1% lower than during LTCS. This result is apparently strange because at a first approach lower ambient temperature is expected to reduce indicated efficiency because of, among other effects, the higher heat transfer. Figure 18 shows some key in-cylinder parameters such as temperature and oxygen concentration at intake valve closing (the key observers to follow the air path changes due to the ambient conditions) and also combustion duration, key parameter effecting the indicated efficiency. As shown, the temperature and oxygen (O2) concentration are higher in ACS than in LTCS. The effect of the temperature is directly related with the ambient temperature, while higher O2 is due to higher EGR with LTCS because the air setting is kept and intake density is higher (the effect is partially compensated in altitude, as later discussed). Higher temperature and O2 concentrations should enhance combustion and lead to shorter durations in ACS. However, this trend is not observed during the initial low part of the WLTC, where combustion duration is slightly higher for ACS. This can be explained because the injection pressure, which is higher for LTCS due to the higher fuel mass injected (Figure 19 top) to compensate mechanical losses. According to the calibration, this has a positive effect specifically in the initial low part of the cycle, where the effect of oxygen is not critical because of low load. Later, as the load increases, thermal and friction differences diminish, relative variation in the injection settings becomes smaller and then ACS shows a shorter average combustion duration, as expected. Hence, after 600 seconds, the combustion of ACS becomes faster than LTCS at 0 m. This combustion performance is affecting the indicated efficiency. However, the effect of the higher fuel injected seems to be the key. As seen in Figure 19 (top), fuel injected is clearly higher for LTCS and thus also the total indicated energy (Figure 19 middle). The ratio between them is the average indicated efficiency (Figure 19 bottom) that is clearly lower for ACS. As stated, the reason justifying this trend is the higher load (in indicated parameters terms) because of the more fuel injected (which is burned faster than in ACS). As the cycle advances, the combustion performance described can also be seen in the indicated efficiency: ACS and LTCS difference tends to diminish.

The noticeable changes can be seen in the heat rejection to coolant and oil along with the heat cumulated in engine structure. There is higher heat accumulation in the material at LTCS conditions because of the low initial temperature of fluids and metal. As the temperature of the material increases, the accumulated energy of the metal decreases, slightly increasing the heat rejected to the coolant. Also, the thermostat opens earlier for ACS, leading to the higher heat transfer. Hence, there is high heat rejection to the coolant at ACS than in LTCS (13% vs 11%). On the other hand, the heat rejection to oil does not show such an important variation (7% in ACS vs 6.7% in LTCS). The final cumulated values of the heat rejected to coolant and oil are slightly higher in ACS

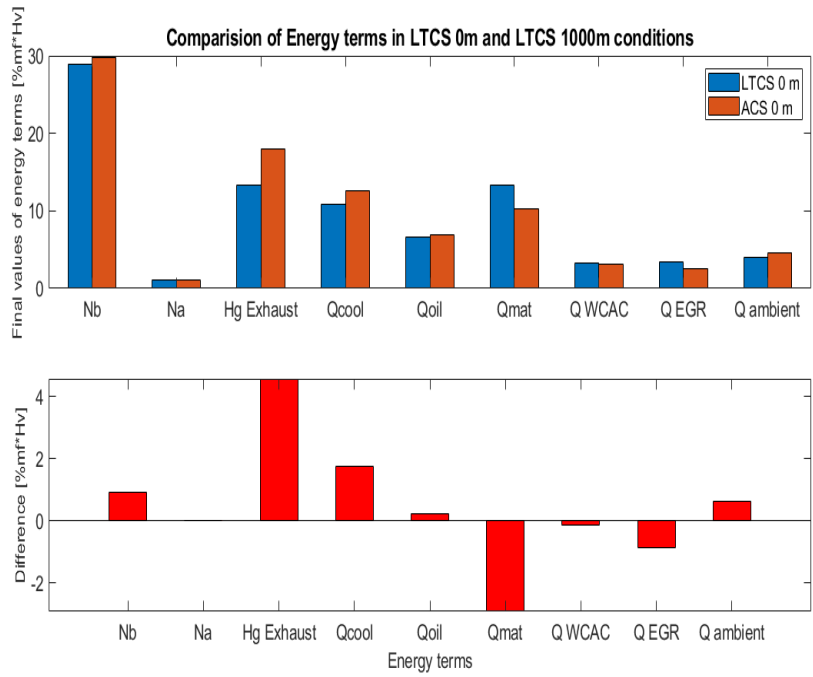

Figure 16. Comparison of energy terms in WLTC in LCTS 0 m and ACS 0 m conditions at the end of the cycle

conditions. Whereas, the heat rejected to material ($\dot{Q}_{mat}$) is higher in LCTS (12.5% vs 10%).

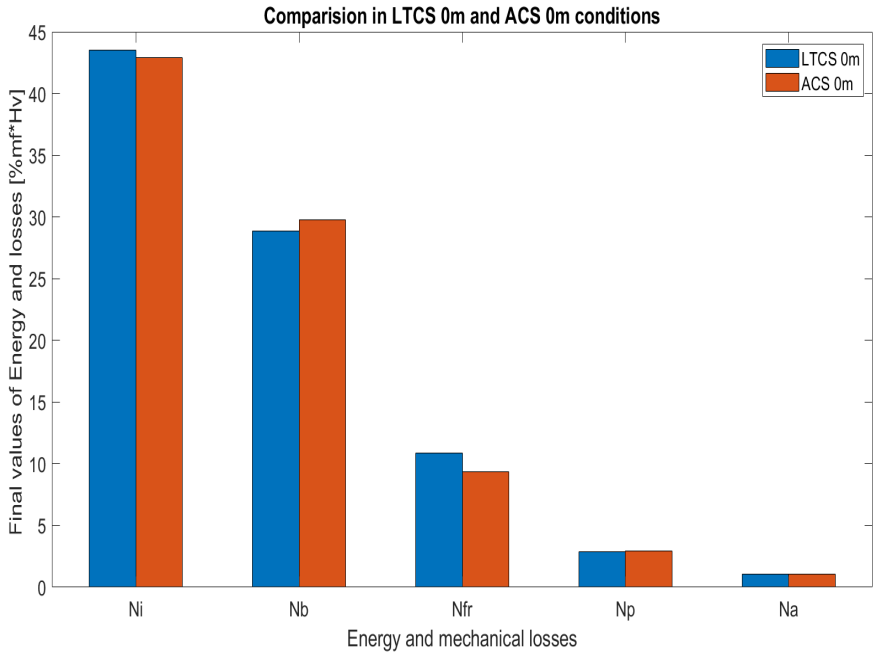

Figure 17. Comparison of energy and losses in WLTC in LCTS 0 m and ACS 0 m conditions

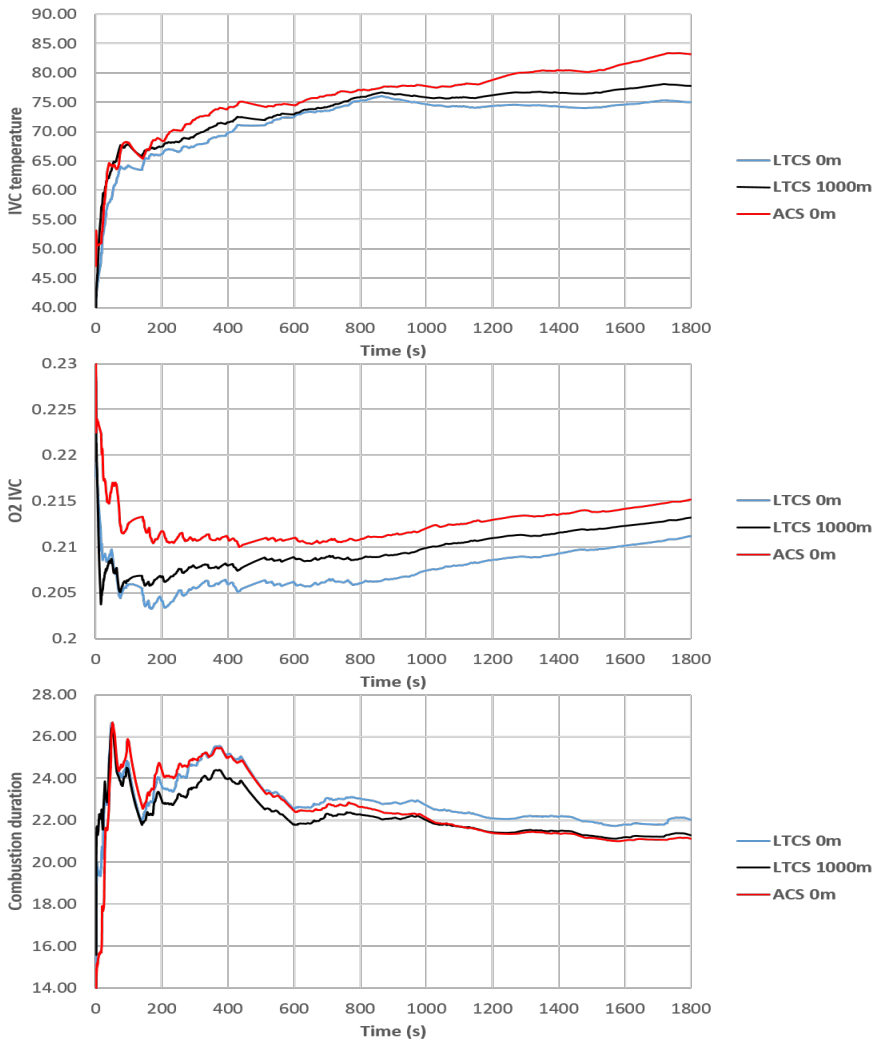

Figure 18. Temperatue at IVC, O2 at IVC and combustion duration in WLTC at LCTS 0 m, LTCS 1000 m and ACS 0 m conditions

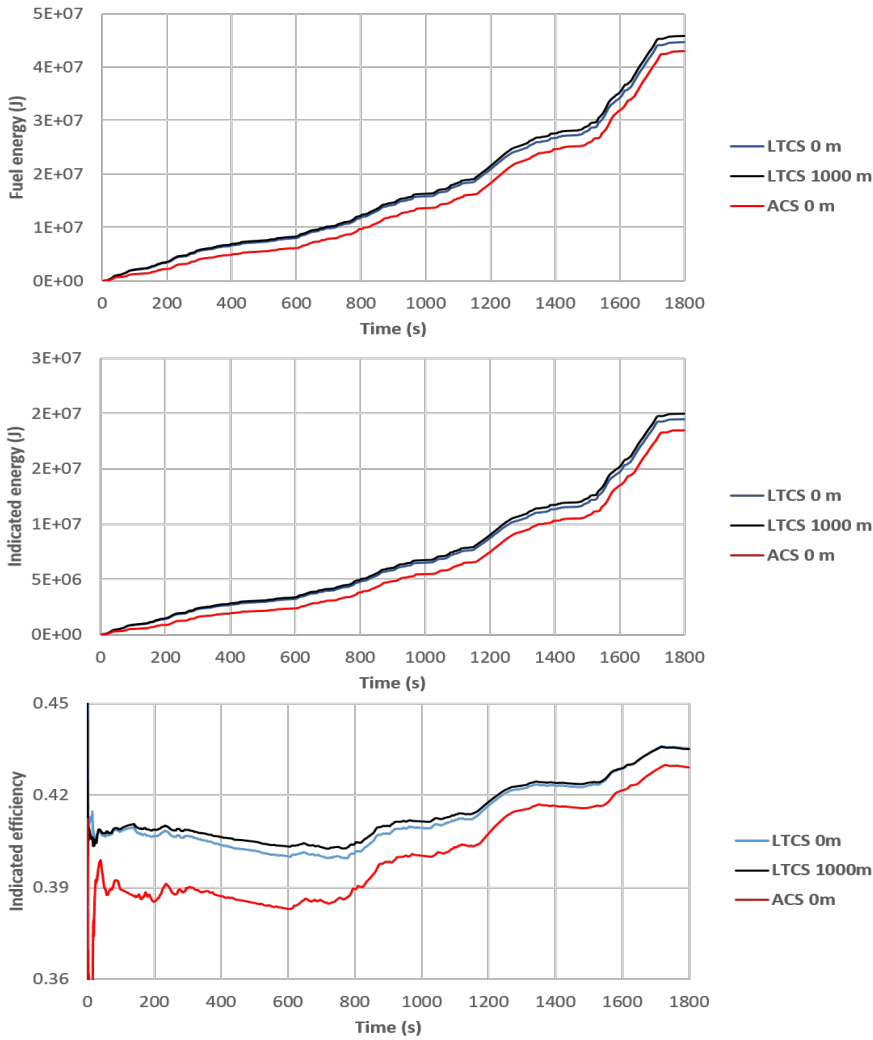

Figure 19. Fuel, indicated energy and indicated efficiency in WLTC at LCTS 0 m, LTCS 1000 m and ACS 0 m conditions

The energy term with higher variation is net exhaust enthalpy, $H_{g,exhaust}$, which is higher in ACS conditions (18% vs 13.5%). This can be considered as a result of the reduction of cumulated heat in the block and lower cumulated EGR in ACS (2.5% vs 3.5%). In the Figure 13, it can be seen that the rejected heat in the LPEGR heat exchanger, $\dot{Q}_{LPEGR}$, is low (less than 1%) when compared to $\dot{Q}_{HPEGR}$. This can be explained by the low temperature at the LPEGR cooler. As shown in Figure 20, despite of only having a net mass flow through the LPEGR cooler during the LPEGR operation, natural convection, pulsing effect and much higher temperature of the gas at the HPEGR cooler, lead to higher heat rejection in it. The rest of the terms, heat rejection in the intercooler, to ambient (pipes, turbo) do not show any important variation.

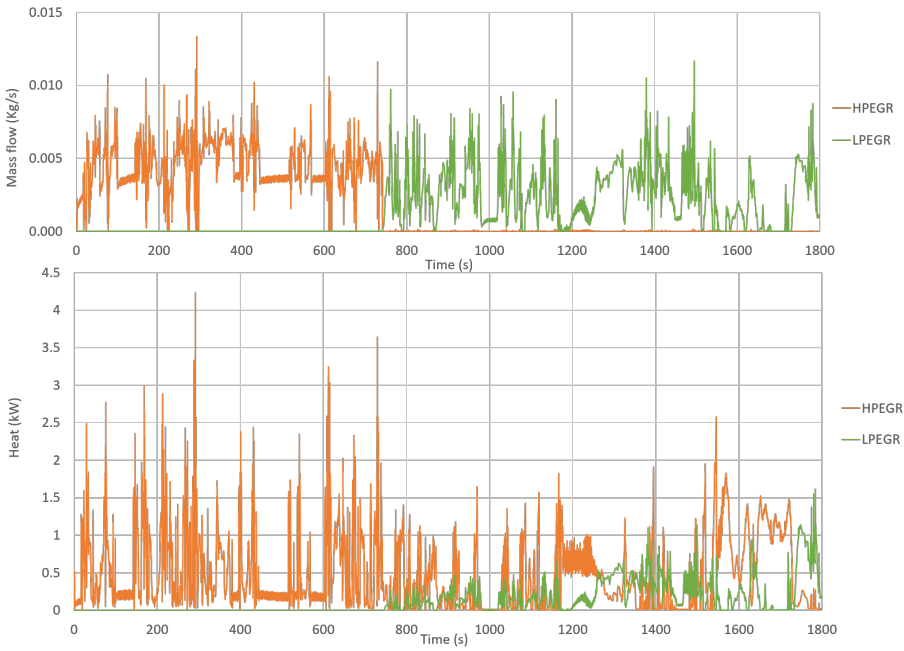

Figure 20. Mass flow and heat at HPEGR and LPEGR in WLTC at ACS conditions

Analysis of altitude effect

After analysing the effect of the starting temperature, this section is devoted to complete the analysis by assessing the effect of altitude in the engine operation. WLTC simulations were launched for LTCS conditions at the altitude of 0 m and 1000 m above the sea level. The LTCS at 0 m is considered the baseline case for the analysis.

Instantaneous energy balances similar to those shown in Figure 9 and 13 were obtained for simulations at altitude of 1000 m. As instantaneous evolution is similar to that presented for LTCS at 0 m, the analysis is going to be focused only on the final results

at the end of the WLTC, to highlight main cumulated differences. In general, it can be observed that differences are small and only one term is changing more than 0.5%. Comparison of energy terms at the end of the WLTC in LTCS at 0 m and 1000 m is shown in Figure 21. It can be seen that cumulated brake efficiency at LTCS 1000 m conditions is slightly lower than LTCS 0 m conditions, but the difference is only about 0.8%. As shown in Figure 22, mean indicated efficiency is similar in both conditions. This can be justified because accordingly to the calibration, VEMOD control follows the same boost pressure target at the two altitudes and thus trapped mass at the inlet valve closing is similar at 0 m and 1000 m. The additional fuel required to reach the demanded torque, even though affecting the combustion process, doesn't affect importantly the indicated performance at the end of the WLTC. As seen in Figure 18, O2 concentration at intake valve closing is slightly higher at 1000 m in comparison to 0 m. This can be explained because the boost pressure is the same, but not the temperature. Due to the higher compression ratio in the compressor, the outlet temperature is higher and hence the intake temperature, thus diminishing EGR (for the same air demand). More O2 and slightly higher temperatures enhance the combustion. As in this case, total fuel is not very different from 0 m, injection settings are similar and thus combustion duration is slightly shorter for 1000 m. This has an effect on indicated efficiency shown in Figure 19 (bottom), where there is a slight higher value at LTCS 1000 m with respect to LTCS 0 m. Hence, the lower mechanical losses during LTCS at 0 m, can be considered as the main reason for the lower brake efficiency. If mechanical losses split is analysed in detail, it can be seen in Figure 22 that both auxiliaries and friction are almost constant because coolant, oil and fuel pumps don't change their operation and oil temperature, main variable for friction, is very similar, as confirmed by the constant heat to oil shown in Figure 21. Thus, the main reason for the brake efficiency diminution is pumping, that increase from 2.9% to 4% of the total fuel energy.

Among the rest of energy terms plotted in Figure 21, there are other two that show a significant increase: heat rejected in the intercooler and coolant heat exchanger. Both of them increase about 0.5%. Heat rejected to the intercooler increases due to the higher compressor outlet temperature because of the higher compression ratio (boost pressure is maintained while compressor inlet pressure is lower due to the ambient conditions). The higher heat rejection to coolant is justified because of the slightly higher intake temperature which is also consequence of higher temperature at the compressor outlet. The rest of variables does not show a remarkable variation.

Having in mind the results discussed in the previous section and here, it can be concluded that the engine response is mainly affected by the ambient temperature while the effect of the altitude is lower.

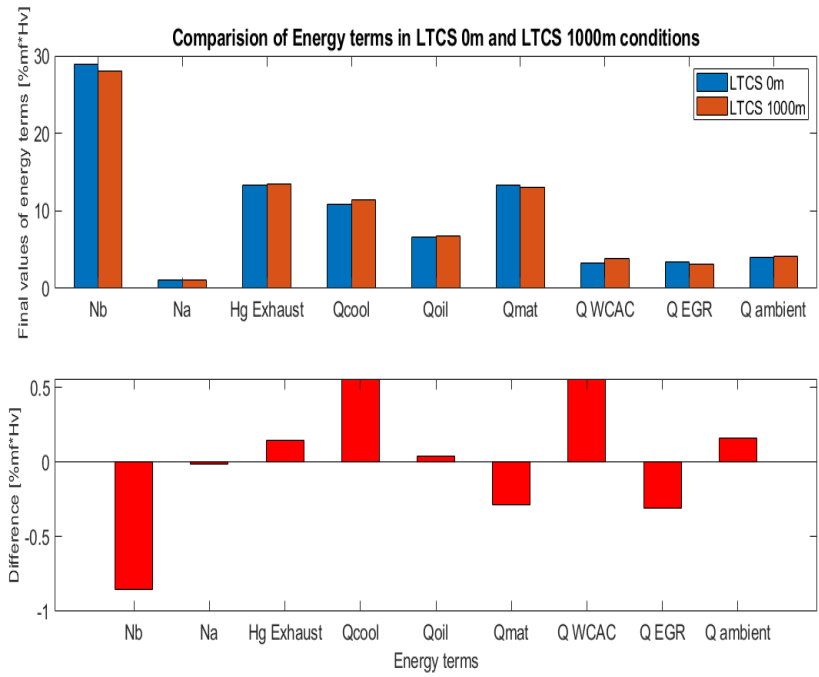

Figure 21. Comparison of energy terms in WLTC in LTCS 0m and LTCS 1000m conditions at the end of the cycle

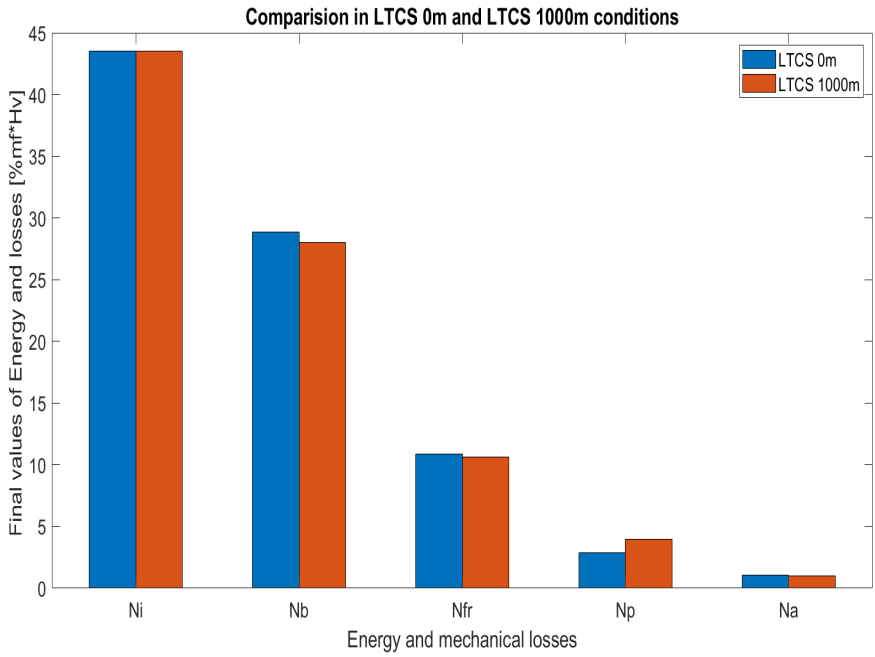

Figure 22. Comparison of energy and losses in WLTC in LTCS 0m and LTCS 1000m conditions at the end of the cycle

Analysis of NOx emissions

Figure 23 shows the NOx at different operating conditions. It can be seen that NOx is higher in LTCS 0 m conditions (with respect to ACS) until around 1300 seconds, and then the trend changes to lower NOx until the end of the cycle. This can be explained with the NOx dependency on temperature and EGR. When the temperature is lower, as air target is kept in the settings, the EGR rate will be higher due to the higher intake density; this should reduce NOx. The higher NOx in LTCS during the initial part of the cycle can be explained because of the higher injected fuel to compensate higher mechanical losses and thus maintaining the torque. However, as the fluid temperature increases along the cycle, the effect of the ambient conditions diminishes (it can be seen in Figure 19 that, in the last part of the cycle, fuel consumption difference between LTCS at 0 m and ACS does not increase) and thus the benefits of LTCS can be seen in NOx in the last part of the WLTC. When comparing LTCS 0 m and LTCS 1000 m, a continuous NOx increase for higher altitude can be seen. The effect can be explained because of the lower EGR rate for 1000 m, as described in the previous section.

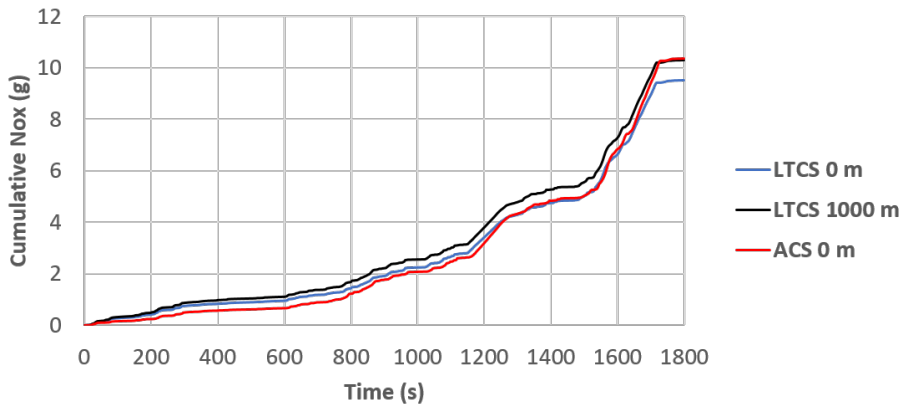

Figure 23. NOx in WLTC at ACS and LTCS conditions

Conclusions

The calibration and validation of the simulation tool, VEMOD have been using a 4-cylinder 1.6 L DI Diesel engine. Key parameters such as pressure, heat released, coolant temperature, oil temperatures and torque have been considered. In both steady-state and transient conditions, a good global performance has been found between the modeled and experimental results.

An extensive analysis of the Global Energy Balance (GEB) has been carried out to assess the effect of various operating conditions on the energy repartition during a transient operation. The GEB was performed considering the complete engine with two starting temperatures : ambient cold start (ACS) and low temperature cold start (LTCS) and two altitudes (0 and 1000 meters).

In all the above mentioned conditions, a "delay" effect due to the unsynchronized phenomena in the gas lines and cylinders has been shown and discussed. This effect diminishes with time, improving the apparent unbalance. It has been shown that the energy balance is reaching around 85% when it was run until 1800 seconds. However, when the simulation is extended, the energy balance reaches about 100%.

It has been shown that at LTCS conditions, the indicated energy is quite stable along the WLTC, while reaching about 44% at the end of the cycle, while brake energy is 29%, showing a clear trend to increase along the WLTC. The lower values of brake energy at the beginning of the operation, can be explained by the higher mechanical losses, being friction the main component, which reaches about 30% of the fuel energy at the start of the WLTC and diminishes to 11% at the end. The higher friction has been justified because of the low oil temperatures during the initial part of WLTC. Also, it has been found that the piston friction is the most important component, accounting for 60% of the total friction losses. Pumping (N_p) and auxiliaries (N_a) are only about 3% and 1% of the fuel energy respectively.

The energy split starting at LTCS conditions has been compared with ACS conditions at 0 m altitude. It has been shown that important changes take place in N_i, N_b, $\dot{Q}_{oil}$, $\dot{Q}_{cool}$ and $\dot{Q}_{mat}$ due to the different initial temperatures in LTCS and ACS conditions. It has been shown that air path changes are affecting IVC conditions both in temperature and composition terms. This is changing the combustion duration, but the main effect is the change of fuel injected, that is leading to operate in LTCS at slightly higher load (from the point of view of in-cylinder conditions). Thus indicated efficiency is lower in ACS. N_b is slightly higher in ACS conditions, when compared to LTCS (30% vs 29%) mainly because of the friction variation. In spite of the small variation in N_b, the fuel consumption increases by 4% in LTCS. It has been seen that $\dot{Q}_{cool}$ is higher in ACS conditions (13% vs 11%) and $\dot{Q}_{oil}$ is higher as well in ACS conditions (7% vs 6.7%). The heat rejected to material ($\dot{Q}_{mat}$) is lower in ACS (12.5% vs 10%). It has been found that the energy term with higher variation is the net exhaust enthalpy, $H_{g,exhaust}$, which is higher in ACS conditions (18% vs 13.5%). The rest of the terms, $\dot{Q}_{WCAC}$, $\dot{Q}_{pipes}$ and $\dot{Q}_{turbo-amb}$ do not show any important variation.

The assessment of altitude was done in LTCS at 0 m and 1000 m. It has been found that apart from the change in pumping and brake energy, the rest of variables does not show a remarkable variation.

The analysis of NOx emissions was done in ACS at 0 m, LTCS at 0 m and 1000 m. It has been found that cumulative NOx is higher in LTCS 0 m when compared to ACS 0 m at the beginning of the cycle, due to the higher fuel required. However, in the last part of the WLTC, NOx has become lower for LTCS 0 m due to the higher EGR achieved. It has been shown that there is a continuous NOx increase for higher altitude when comparing LTCS at 0 m and 1000 m because of the lower EGR rate due to the slightly higher intake temperature, that is also promoting NOx formation.

As a brief summary, it can be concluded that reducing ambient temperature from 20°C to -7°C decreases brake efficiency by 1% mainly due to the higher friction. The effect of increasing altitude 1000 m decreases brake efficiency by 0.8% in the WLTC because of the change in the pumping, while the fuel consumption increases by 2.5%. Altitude does not seem to have any important effect on the rest of the energy terms. However, different inital temperatures are majorly effecting the exhaust enthalpy, heat rejected to coolant and heat accumulated in the block as discussed.

Acknowledgments

This research has been partially funded by the European Union's Horizon 2020 Framework Programme for research, technological development and demonstration under grant agreement 723976 ("DiePeR") and by the Spanish government under the grant agreement TRA2017-89894-R ("MECOEM") and Sushma Artham was supported by FPI grant with reference PRE2018-084411. The authors wish to thank Renault SAS, especially P. Mallet and E. Gaïffas, for supporting this research.

References

1. E J, Liu T, Yang W et al. A skeletal mechanism modeling on soot emission characteristics for biodiesel surrogates with varying fatty acid methyl esters proportion. *Applied Energy* 2016; 181: 322–331. DOI:10.1016/j.apenergy.2016.08.090. URL http://dx.doi.org/10.1016/j.apenergy.2016.08.090.
2. Wu G, Lu Z, Xu X et al. Numerical investigation of aeroacoustics damping performance of a Helmholtz resonator: Effects of geometry, grazing and bias flow. *Aerospace Science and Technology* 2019; 86: 191–203. DOI:10.1016/j.ast.2019.01.007.
3. Li Y, Chen Y, Wu G et al. Experimental evaluation of water-containing isopropanol-n-butanol-ethanol and gasoline blend as a fuel candidate in spark-ignition engine. *Applied Energy* 2018; 219(March): 42–52. DOI:10.1016/j.apenergy.2018.03.051. URL https://doi.org/10.1016/j.apenergy.2018.03.051.
4. Giakoumis EG. A statistical investigation of biodiesel effects on regulated exhaust emissions during transient cycles. *Applied Energy* 2012; 98: 273–291. DOI:10.1016/j.apenergy.2012.03.037. URL http://dx.doi.org/10.1016/j.apenergy.2012.03.037.

5. Triantafyllopoulos G, Katsaounis D, Karamitros D et al. Experimental assessment of the potential to decrease diesel NOx emissions beyond minimum requirements for Euro 6 Real Drive Emissions (RDE) compliance. *Science of the Total Environment* 2018; 618(x): 1400–1407. DOI:10.1016/j.scitotenv.2017.09.274. URL https://doi.org/10.1016/j.scitotenv.2017.09.274.
6. Park H, Bae C and Ha C. A comprehensive analysis of multiple injection strategies for improving diesel combustion process under cold-start conditions. *Fuel* 2019; 255(June): 115762. DOI:10.1016/j.fuel.2019.115762. URL https://doi.org/10.1016/j.fuel.2019.115762.
7. E J, Han D, Deng Y et al. Performance enhancement of a baffle-cut heat exchanger of exhaust gas recirculation. *Applied Thermal Engineering* 2018; 134(January): 86–94. DOI:10.1016/j.applthermaleng.2018.01.109. URL https://doi.org/10.1016/j.applthermaleng.2018.01.109.
8. Jiaqiang E, Zhao X, Xie L et al. Performance enhancement of microwave assisted regeneration in a wall-flow diesel particulate filter based on field synergy theory. *Energy* 2019; 169: 719–729. DOI:10.1016/j.energy.2018.12.086.
9. Jiaqiang E, Liu G, Zhang Z et al. Effect analysis on cold starting performance enhancement of a diesel engine fueled with biodiesel fuel based on an improved thermodynamic model. *Applied Energy* 2019; 243(March): 321–335. DOI:10.1016/j.apenergy.2019.03.204. URL https://doi.org/10.1016/j.apenergy.2019.03.204.
10. Ramadhas AS and Xu H. Improving Cold Start and Transient Performance of Automotive Diesel Engine at Low Ambient Temperatures. *SAE Technical Papers* 2016; 2016-April(April). DOI:10.4271/2016-01-0826.
11. Rakopoulos CD, Dimaratos AM, Giakoumis EG et al. Investigating the emissions during acceleration of a turbocharged diesel engine operating with bio-diesel or n-butanol diesel fuel blends. *Energy* 2010; 35(12): 5173–5184. DOI:10.1016/j.energy.2010.07.049. URL http://dx.doi.org/10.1016/j.energy.2010.07.049.
12. D Rakopoulos, Evangelos G Giakoumis. *Diesel Engine Transient Operation - Principles of Operation and Simulation Analysis*. ISBN 9781848823747.
13. Rakopoulos CD, Giakoumis EG, Hountalas DT et al. The Effect of Various Dynamic, Thermodynamic and Design Parameters on the Performance of a Turbocharged Diesel Engine Operating under Transient Load Conditions. *SAE Technical Paper Series* 2010; 1(724). DOI: 10.4271/2004-01-0926.
14. European Parliament and Council of the European Union. Regulation (EC) No 852/2004 of the European Parliament and of the Council. *Official Journal of the European Communities* 2004; 2006(December 2006): 1–54. URL http://eur-lex.europa.eu/LexUriServ/LexUriServ.do?uri=OJ:L:2004:139:0001:0054:en:PDF.
15. Martin J, Arnau F, Piqueras P et al. Development of an Integrated Virtual Engine Model to Simulate New Standard Testing Cycles. *SAE Technical Paper Series* 2018; 1: 1–17. DOI: 10.4271/2018-01-1413.
16. Payri F, Lopez JJ, Pla B et al. Assessing the Limits of Downsizing in Diesel Engines. *SAE Technical Paper Series* 2014; 1. DOI:10.4271/2014-32-0128.
17. Giakoumis EG, Rakopoulos CD, Dimaratos AM et al. Exhaust emissions of diesel engines operating under transient conditions with biodiesel fuel blends. *Progress in Energy and*

Combustion Science 2012; 38(5): 691–715. DOI:10.1016/j.pecs.2012.05.002. URL http://dx.doi.org/10.1016/j.pecs.2012.05.002.

18. Cui Y, Deng K and Wu J. A direct injection diesel combustion model for use in transient condition analysis. *Proceedings of the Institution of Mechanical Engineers, Part D: Journal of Automobile Engineering* 2001; 215(9): 995–1004. DOI:10.1243/0954407011528563.
19. Pamminger Michael CMHRVWT Wang Buyu. The impact of water injection and exhaust gas recirculation on combustion and emissions in a heavy-duty compression ignition engine operated on diesel and gasoline. *INTERNATIONAL JOURNAL OF ENGINE RESEARCH* 2020; 21. DOI:10.1177/1468087418815290.
20. Tauzia X, Maiboom A, Karaky H et al. Experimental analysis of the influence of coolant and oil temperature on combustion and emissions in an automotive diesel engine. *International Journal of Engine Research* 2019; 20(2): 247–260. DOI:10.1177/1468087417749391.
21. Cárdenas MD, Gómez A and Armas O. Pollutant emissions from starting a common rail diesel engine fueled with different biodiesel fuels. *Journal of Energy Engineering* 2016; 142(2). DOI:10.1061/(ASCE)EY.1943-7897.0000328.
22. Giakoumis EG, Dimaratos AM, Rakopoulos CD et al. Combustion Instability during Starting of Turbocharged Diesel Engine Including Biofuel Effects. *Journal of Energy Engineering* 2017; 143(2). DOI:10.1061/(ASCE)EY.1943-7897.0000402.
23. García-Contreras R, Armas O, Mata C et al. Impact of Gas To Liquid and diesel fuels on the engine cold start. *Fuel* 2017; 203: 298–307. DOI:10.1016/j.fuel.2017.04.116.
24. Dardiotis C, Martini G, Marotta A et al. Low-temperature cold-start gaseous emissions of late technology passenger cars. *Applied Energy* 2013; 111: 468–478. DOI:10.1016/j.apenergy.2013.04.093. URL http://dx.doi.org/10.1016/j.apenergy.2013.04.093.
25. Tinprabath P, Hespel C, Chanchaona S et al. Influence of biodiesel and diesel fuel blends on the injection rate under cold conditions. *Fuel* 2015; 144: 80–89. DOI:10.1016/j.fuel.2014.12.010. URL http://dx.doi.org/10.1016/j.fuel.2014.12.010.
26. Park H, Shin J and Bae C. Spray and Combustion of Diesel Fuel under Simulated Cold-Start Conditions at Various Ambient Temperatures. In *SAE Technical Paper*. SAE International. DOI:10.4271/2017-24-0069. URL https://doi.org/10.4271/2017-24-0069.
27. Roberts A, Brooks R and Shipway P. Internal combustion engine cold-start efficiency: A review of the problem, causes and potential solutions. *Energy Conversion and Management* 2014; 82: 327–350. DOI:10.1016/j.enconman.2014.03.002. URL http://dx.doi.org/10.1016/j.enconman.2014.03.002.
28. Horng RF and Chou HM. Effect of input energy on the emission of a motorcycle engine with an electrically heated catalyst in cold-start conditions. *Applied Thermal Engineering* 2004; 24(14-15): 2017–2028. DOI:10.1016/j.applthermaleng.2004.02.005.
29. Clairotte M, Adam TW, Zardini AA et al. Effects of low temperature on the cold start gaseous emissions from light duty vehicles fuelled by ethanol-blended gasoline. *Applied Energy* 2013; 102(2013): 44–54. DOI:10.1016/j.apenergy.2012.08.010. URL http://dx.doi.org/10.1016/j.apenergy.2012.08.010.
30. Chen RH, Chiang LB, Chen CN et al. Cold-start emissions of an SI engine using ethanol-gasoline blended fuel. *Applied Thermal Engineering* 2011; 31(8-9): 1463–1467. DOI:10.1016/j.applthermaleng.2011.01.021. URL http://dx.doi.org/10.1016/j.applthermaleng.2011.01.021.

31. Gumus M. Reducing cold-start emission from internal combustion engines by means of thermal energy storage system. *Applied Thermal Engineering* 2009; 29(4): 652–660. DOI:10.1016/j.applthermaleng.2008.03.044. URL http://dx.doi.org/10.1016/j.applthermaleng.2008.03.044.
32. Deng Y, Liu H, Zhao X et al. Effects of cold start control strategy on cold start performance of the diesel engine based on a comprehensive preheat diesel engine model. *Applied Energy* 2018; 210(October 2017): 279–287. DOI:10.1016/j.apenergy.2017.10.093. URL http://dx.doi.org/10.1016/j.apenergy.2017.10.093.
33. Luján JM, Dolz V, Monsalve-Serrano J et al. High-pressure exhaust gas recirculation line condensation model of an internal combustion diesel engine operating at cold conditions. *International Journal of Engine Research* 2019; DOI:10.1177/1468087419868026.
34. Luján JM, Climent H, Ruiz S et al. Influence of ambient temperature on diesel engine raw pollutants and fuel consumption in different driving cycles. *International Journal of Engine Research* 2019; 20(8-9): 877–888. DOI:10.1177/1468087418792353.
35. Galindo J, Dolz V, Monsalve-Serrano J et al. Advantages of using a cooler bypass in the low-pressure exhaust gas recirculation line of a compression ignition diesel engine operating at cold conditions. *International Journal of Engine Research* 2020; : 1–12DOI: 10.1177/1468087420914725.
36. Kawaguchi A, Wakisaka Y, Nishikawa N et al. Thermo-swing insulation to reduce heat loss from the combustion chamber wall of a diesel engine. *International Journal of Engine Research* 2019; 20(7): 805–816. DOI:10.1177/1468087419852013.
37. Liu S, Shen L, Bi Y et al. Effects of altitude and fuel oxygen content on the performance of a high pressure common rail diesel engine. *Fuel* 2014; 118: 243–249. DOI:10.1016/j.fuel.2013.10.007. URL http://dx.doi.org/10.1016/j.fuel.2013.10.007.
38. Payri F, Olmeda P, Martin J et al. A New Tool to Perform Global Energy Balances in DI Diesel Engines. *SAE International Journal of Engines* 2014; 7(1): 43–59. DOI: 10.4271/2014-01-0665.
39. Payri F, Martin J, Garcia A et al. Experimental and Theoretical Analysis of the Energy Balance in a DI Diesel Engine. *SAE Technical Paper Series* 2015; 1(x). DOI:10.4271/2015-01-1651.
40. Tauzia X and Maiboom A. Experimental study of an automotive Diesel engine efficiency when running under stoichiometric conditions. *Applied Energy* 2013; 105: 116–124. DOI:10.1016/j.apenergy.2012.12.034. URL http://dx.doi.org/10.1016/j.apenergy.2012.12.034.
41. Abedin MJ, Masjuki HH, Kalam MA et al. Energy balance of internal combustion engines using alternative fuels. *Renewable and Sustainable Energy Reviews* 2013; 26: 20–33. DOI: 10.1016/j.rser.2013.05.049. URL http://dx.doi.org/10.1016/j.rser.2013.05.049.
42. Ajav EA, Singh B and Bhattacharya TK. Thermal balance of a single cylinder diesel engine operating on alternative fuels. *Energy Conversion and Management* 2000; 41(14): 1533–1541. DOI:10.1016/S0196-8904(99)00175-2.
43. Durgun O and Şahin Z. Theoretical investigation of heat balance in direct injection (DI) diesel engines for neat diesel fuel and gasoline fumigation. *Energy Conversion and Management* 2009; 50(1): 43–51. DOI:10.1016/j.enconman.2008.09.007.

44. Smith LA, Preston WH, Dowd G et al. Application of a First Law Heat Balance Method to a Turbocharged Automotive Diesel Engine. *SAE Technical Paper Series* 2010; 1. DOI: 10.4271/2009-01-2744.
45. Olmeda P, Martín J, Novella R et al. Assessing the optimum combustion under constrained conditions. *International Journal of Engine Research* 2018; : 1–13DOI:10.1177/1468087418814086.
46. Taymaz I. An experimental study of energy balance in low heat rejection diesel engine. *Energy* 2006; 31(2-3): 364–371. DOI:10.1016/j.energy.2005.02.004.
47. Jung D, Yong J, Choi H et al. Analysis of engine temperature and energy flow in diesel engine using engine thermal management, 2013. DOI:10.1007/s12206-012-1235-4.
48. Caresana F, Bilancia M and Bartolini CM. Numerical method for assessing the potential of smart engine thermal management: Application to a medium-upper segment passenger car. *Applied Thermal Engineering* 2011; 31(16): 3559–3568. DOI:10.1016/j.applthermaleng.2011.07.017. URL http://dx.doi.org/10.1016/j.applthermaleng.2011.07.017.
49. Payri F, López JJ, Martín J et al. Improvement and application of a methodology to perform the Global Energy Balance in internal combustion engines. Part 1: Global Energy Balance tool development and calibration. *Energy* 2018; 152: 666–681. DOI:10.1016/j.energy.2018.03.118.
50. Romero CA, Torregrosa A, Olmeda P et al. Energy Balance During the Warm-Up of a Diesel Engine. *SAE Technical Paper Series* 2014; 1. DOI:10.4271/2014-01-0676.
51. Kan Z, Hu Z, Lou D et al. Effects of altitude on combustion and ignition characteristics of speed-up period during cold start in a diesel engine. *Energy* 2018; 150: 164–175. DOI:10.1016/j.energy.2017.12.103.
52. Olmeda P, Martín J, Arnau FJ et al. Analysis of the energy balance during World harmonized Light vehicles Test Cycle in warmed and cold conditions using a Virtual Engine. *International Journal of Engine Research* 2019; DOI:10.1177/1468087419878593.
53. Olmeda P, Martin J, Garcia A et al. Evaluation of EGR Effect on the Global Energy Balance of a High Speed DI Diesel Engine. *SAE Technical Paper Series* 2016; 1. DOI: 10.4271/2016-01-0646.
54. Benajes J, Olmeda P, Martín J et al. A new methodology for uncertainties characterization in combustion diagnosis and thermodynamic modelling. *Applied Thermal Engineering* 2014; 71(1): 389–399. DOI:10.1016/j.applthermaleng.2014.07.010.
55. Payri F, Margot X, Gil A et al. Computational Study of Heat Transfer to the Walls of a DI Diesel Engine. *SAE Technical Paper Series* 2010; 1(724). DOI:10.4271/2005-01-0210.
56. Payri F, Olmeda P, Martín J et al. Experimental analysis of the global energy balance in a di diesel engine. *Applied Thermal Engineering* 2015; 89(x): 545–557. DOI:10.1016/j.applthermaleng.2015.06.005.
57. Payri F, López JJ, Martín J et al. Improvement and application of a methodology to perform the Global Energy Balance in internal combustion engines. Part 1: Global Energy Balance tool development and calibration. *Energy* 2018; 152: 666–681. DOI:10.1016/j.energy.2018.03.118.
58. Carreño Arango R. *A comprehensive methodology to analyse the Global Energy Balance in Reciprocating Internal Combustion Engines*. September 2016.

59. Olmeda P, Dolz V, Arnau FJ et al. Determination of heat flows inside turbochargers by means of a one dimensional lumped model. *Mathematical and Computer Modelling* 2013; 57(7-8): 1847–1852. DOI:10.1016/j.mcm.2011.11.078. URL http://dx.doi.org/10.1016/j.mcm.2011.11.078.
60. Torregrosa A, Olmeda P, Degraeuwe B et al. A concise wall temperature model for di Diesel engines. *Applied Thermal Engineering* 2006; 26(11-12): 1320–1327. DOI:10.1016/j.applthermaleng.2005.10.021.
61. Jose M Desantes JJLAC Jean Arregle. Scaling laws for free turbulent gas jets and Diesel like sprays, Atomization and Sprays 16. *Atomization and Sprays* 2006; 16: 443–474. DOI: 10.1615/AtomizSpr.v16.i4.60.
62. Vasileios Hamosfakidis RR. Optimization of a hydrocarbon fuel ignition model for two single component surrogates of diesel fuel. *Combustion and Flame* 2003; 132. DOI: 10.1016/S0010-2180(02)00489-3.

-